

Functional Regression on Manifold with Contamination

Zhenhua Lin* Fang Yao †

Abstract

We propose a new perspective on functional regression with a predictor process via the concept of manifold that is intrinsically finite-dimensional and embedded in an infinite-dimensional functional space, where the predictor is contaminated with discrete/noisy measurements. By a method of functional local linear manifold smoothing, we achieve a polynomial rate of convergence that adapts to the intrinsic manifold dimension and the level of sampling/noise contamination with a phase transition phenomenon depending on their interplay. This is in contrast to the logarithmic convergence rate in the literature of functional nonparametric regression. We demonstrate that the proposed method enjoys favorable finite sample performance relative to commonly used methods via simulated and real data examples.

Keywords: Contaminated functional data, functional nonparametric regression, intrinsic dimension, local linear manifold smoothing, phase transition

*Department of Statistics, University of California at Davis.

†Department of Statistical Sciences, University of Toronto.

1 Introduction

Regression with a functional predictor is of central importance in the field of functional data analysis, the field that has been advanced by Ramsay and Silverman (1997) and Ramsay and Silverman (2002), among other researchers. Early development of functional regression focuses on functional linear models, such as Cardot *et al.* (1999), Yao *et al.* (2005b), Hall and Horowitz (2007), and Yuan and Cai (2010). Extensions of linear models include generalized linear regression by Cardot and Sarda (2005) and Müller and Stadtmüller (2005), additive model by Müller and Yao (2008), quadratic model by Yao and Müller among many others. These works prescribe some specific forms of the regression model, and may be regarded as functional “parametric” regression models (Ferraty and Vieu, 2006) which often entail an efficient estimation procedure and hence are well studied in the literature.

In contrast, functional “nonparametric” regression that does not impose structural constraints on the regression function receives relatively less attention. The first landmark development of nonparametric functional data analysis is the monograph of Ferraty and Vieu (2006). Recent advances on functional nonparametric regression include Nadaraya-Watson estimator studied by Ferraty *et al.* (2012), and k -nearest-neighbor (k NN) estimators investigated by Kudraszow and Vieu (2013). The development of functional nonparametric regression is hindered by a theoretical barrier that is formulated in Mas (2012) and is linked to the small ball probability problem (Delaigle and Hall, 2010). Essentially, it is shown that in a rather general setting, the minimax rate of nonparametric regression on a generic functional space is slower than any polynomial of sample size, as opposite to functional parametric regression (e.g. Hall and Horowitz, 2007; Yuan and Cai, 2010, for functional linear regression). These endeavors on functional nonparametric regression do not explore the intrinsic structures that are not uncommon in practice. However, it is suggested in Chen and Müller (2012) that functional data often possess a low-dimensional manifold structure which can be utilized for more efficient representation. By contrast, we consider to explore *nonlinear* low-dimensional structures for functional nonparametric regression.

Specifically, we study Functional REgression on Manifolds (FREM), a model given by

$$Y = g(X) + \varepsilon, \quad (1)$$

where Y is a scalar response, X is a functional predictor sampled from an unknown manifold \mathcal{M} , ε is the error term that is independent of X , and g is some unknown functional that is to be estimated. In reality, the functional predictor X is rarely fully observed. To accommodate this common practice, we assume X is recorded at a grid of points with noise.

The FREM model features a manifold structure \mathcal{M} that underlies the functional predictor X and is embedded in the functional space $\mathcal{L}^2(D)$, the space of square integrable functions defined on a compact domain $D \subset \mathbb{R}$. For a background on manifolds, we refer readers to Lang (1995) and Lang (1999). Although data analysis with manifold structures has been studied in the statistical literature (e.g., Aswani *et al.*, 2011; Cornea *et al.*, 2017; Yuan *et al.*, 2012), the literature relating functional data to manifolds is scarce. Chen and Müller (2012) considers the representation of functional data on a manifold that has only one chart and hence is essentially a linear manifold. Zhou and Pan (2014) investigates functional principal component analysis on an irregular planar domain which can be viewed as a linear manifold as well. Mostly related to our work is Lila and Aston (2016) that models functions sampled from a nonlinear two-dimensional manifold and focuses on the principal component analysis. To the best of our knowledge, we are the first to consider a nonlinear manifold structure in the setting of functional regression where a *global* representation of X living in a nonlinear low-dimensional space can be inefficient. For illustration, we provide Example 1 in the appendix, where a random process takes values in a *one-dimensional* manifold embedded in $\mathcal{L}^2([0, 1])$ while has an *infinite* number of components in its Karhunen-Loève expansion.

When estimating the regression functional g in (1), we explicitly account for the hidden manifold structure by estimating the tangent spaces of the manifold. Tangent space based estimation methods are common in the analysis of multivariate data with a manifold structure. For example,

Aswani *et al.* (2011) utilizes the tangent structure for regularization on regression with collinear predictors. To the best of our knowledge, this article is the first to explore tangent space based methods for functional regression analysis. Specifically, we first recover the observed functional predictors from their discrete/noisy measurements, and then adopt the local linear manifold smoothing acting on tangent spaces proposed by Cheng and Wu (2013) (referred as MALLER hereafter as in their paper) to study manifold regression of Euclidean data. While FREM and MALLER share the same intrinsic aspect of the manifold setup, they fundamentally differ in the ambient aspect, which raises challenging issues unique to functional data. First, functional data naturally live in an *infinite-dimensional* ambient space, while the Euclidean data considered by Cheng and Wu (2013) have finite ambient dimension.

The infinite dimensionality poses significant challenge on theoretical analysis of the estimated intrinsic dimension and tangent spaces. To appreciate this, for example, it is nontrivial to establish Lemma S.9 and S.10 (given in the Supplementary Material) which are critical for determining the convergence rate of the estimated tangent spaces, as these lemmas involve derivation of tight uniform bounds for some infinite sequences of variables tied to the ambiently infinite dimensionality of functional data,

while such bounds are relatively straightforward for a *finite* sequence in Cheng and Wu (2013). Hence the results in Cheng and Wu (2013) are not applicable in our analysis.

Second, the effect of noise/sampling in the observed functional data needs to be explicitly accounted, since functional data are discretely and noisily recorded in practice, which then introduces contamination on the functional predictor. This contamination issue is not encountered in Cheng and Wu (2013), or is only considered in the context of linear regression of multivariate data (Aswani *et al.*, 2011; Loh and Wainwright, 2012). Although the smoothness nature of functional data makes it possible to recover functional predictors from their discrete/noisy measurements, the contamination persists (it might decay with a growing sample size, but does not disappear completely) and lives in the *ambient* space (since the manifold is unknown, it is difficult to utilize its information for function recovery). We are now faced with the conundrum that, the unobservable

functional predictor being on a low-dimensional manifold, we only have its (infinite-dimensional) contaminated surrogate for regression. Coupled with the infinite dimensionality of the ambient space, it is unclear whether the intrinsic dimension can be consistently estimated, whether the local manifold structure can be well approximated, and whether the theoretical barrier (Mas, 2012) can be bypassed with such contaminated functional predictors. It is the primary goal of our paper to answer these questions and tackle the challenging issues of an infinite-dimensional ambient space and contamination on the functional predictors in the presence of an intrinsic low-dimensional manifold structure. As such, our development here is distinct from Cheng and Wu (2013) which aims at dimension reduction for multivariate data and assumes fully observed predictors without noise.

The main contributions of this article are as follows. First, by exploring structural information of the predictor, FREM entails an effective estimation procedure that adapts to the manifold structure and the contamination level while maintaining the flexibility of functional nonparametric regression. We stress that the underlying embedded manifold is unknown, and we do not require knowledge of the manifold to construct our estimator. Second, by careful theoretical analysis, we confirm that the regression functional g can be estimated at a polynomial convergence rate of the sample size, especially when only the contaminated functional predictors are available. This provides a new angle to functional nonparametric regression that does not utilize intrinsic structure and is subject to the theoretical barrier of logarithmic rates (Mas, 2012). Third, the contamination on predictors is explicitly taken into account and the level of contamination is shown to be an integrated part of the convergence rate, which has not been well studied even in classical functional linear regression, e.g., Hall and Horowitz (2007) is based on fully observed functions and Kong *et al.* (2016) asymptotically ignores the error induced by pre-smoothing densely observed functions. Finally, we discover that, the polynomial convergence rate exhibits a phase transition phenomenon, depending on the interplay between the intrinsic dimension of the manifold and the contamination level in the predictor. This type of phase transition in functional regression has not yet been studied, and is distinct from those concerning estimation of mean/covariance functions for functional data (e.g. Cai and Yuan, 2011; Zhang and Wang, 2016). In addition, during our theoretical development, we obtain some results

that are generally useful with their own merit, such as the consistent estimation for the intrinsic dimension and the tangent spaces of the manifold that underlies the contaminated functional data.

We organize the rest of the paper as follows. In Section 2, we describe the estimation procedure for FREM. The theoretical properties of the proposed method are presented in Section 3. Numerical evidence via simulation studies is provided in Section 4, followed by real data examples in Section 5. Proofs of main theorems are deferred to the Appendix, while some auxiliary results and technical lemmas with proofs are placed in the online Supplementary Material for space economy.

2 Estimation of FREM

To estimate the functional g in model (1) based on an independently and identically distributed (i.i.d.) sample $\{(X_i, Y_i)\}_{i=1}^n$ of size n , we assume that each predictor X_i is observed at m_i design points $T_{i1}, T_{i2}, \dots, T_{im_i} \in D$. Here, we consider a random design of T_{ij} , where T_{ij} are i.i.d. sampled from a density f_T . We should point out that our method and theory in this article apply to the fixed design with slight modification. Denote the observed values at the T_{ij} by $X_{ij}^* = X_i(T_{ij}) + \zeta_{ij}$, where ζ_{ij} are random noise with mean zero and independent of all X_i and T_{ij} . Let $\mathbb{X}_i = \{(T_{i1}, X_{i1}^*), (T_{i2}, X_{i2}^*), \dots, (T_{im_i}, X_{im_i}^*)\}$, which represents all measurements for the realization X_i , and $\mathcal{X} = \{\mathbb{X}_1, \mathbb{X}_2, \dots, \mathbb{X}_n\}$ constitutes the observed data for the functional predictor. At this point, we shall clarify that, although each trajectory X_i as a whole function resides on the manifold \mathcal{M} , its discrete values $X_i(T_{ij})$ (or the noise version X_{ij}^*) as real numbers do not. Neither does each m_i -dimensional vector $\mathbb{V}_i = (X_i(T_{i1}), \dots, X_i(T_{im_i}))$ or $\mathbb{V}_i^* = (X_{i1}^*, \dots, X_{im_i}^*)$. As \mathbb{V}_i are multi-dimensional vectors, one might think of the model $Y_i = g^{\text{MALLER}}(\mathbb{V}_i) + \varepsilon_i$ and applying the MALLER estimator from Cheng and Wu (2013), which is in fact not applicable. First, the vector \mathbb{V}_i does not necessarily have a low-dimensional structure, so that the manifold assumption on \mathbb{V}_i in Cheng and Wu (2013) may not hold. Second, the number m_i may vary from subject to subject and hence vectors \mathbb{V}_i live in different Euclidean spaces, while MALLER requires samples of the

predictor to be from the same Euclidean space. Third, even when $m_i \equiv m$ for all i , the observation time points $\mathbb{T}_i = \{T_{i1}, \dots, T_{im_i}\}$ can be different across subjects, so that the regression function g^{MALLER} depends on \mathbb{T}_i and also i , while Cheng and Wu (2013) implicitly requires g^{MALLER} to be independent of subjects. Similar argument applies to the noisy version \mathbb{V}_i^* as well.

We first recover each function X_i based on the observed data \mathcal{X} by individual smoothing estimation. Here we do not consider the case of sparsely observed functions when only a few noisy measurements are available for each subject (Yao *et al.*, 2005a,b), due to the elevated challenge of estimating the unknown manifold structure, which can be a topic for further investigation. Commonly used techniques include local linear smoother (Fan, 1993) and spline smoothing (Ramsay and Silverman, 2005), among others. By applying any smoothing method, we obtain the estimated \hat{X}_i of X_i , referred to as the contaminated version of X_i that are used in subsequent steps to estimate g at any given $x \in \mathcal{M}$. To be specific, we consider the local linear estimate of $X_i(t)$ given by \hat{b}_1 with

$$(\hat{b}_1, \hat{b}_2) = \arg \min_{(b_1, b_2) \in \mathbb{R}^2} \frac{1}{m_i} \sum_{j=1}^{m_i} \{X_{ij}^* - b_1 - b_2(T_{ij} - t)\}^2 K\left(\frac{T_{ij} - t}{h_i}\right), \quad (2)$$

where K is a compactly supported symmetric density function and h_i is the bandwidth, leading to

$$\hat{b}_1 = \frac{R_0 S_2 - R_1 S_1}{S_0 S_2 - S_1^2}, \quad (3)$$

where for $r = 0, 1$ and 2 ,

$$S_r(t) = \frac{1}{m_i h_i} \sum_{j=1}^{m_i} K\left(\frac{T_{ij} - t}{h_i}\right) \left(\frac{T_{ij} - t}{h_i}\right)^r, \quad R_r(t) = \frac{1}{m_i h_i} \sum_{j=1}^{m_i} K\left(\frac{T_{ij} - t}{h_i}\right) \left(\frac{T_{ij} - t}{h_i}\right)^r X_{ij}^*.$$

One technical issue with the estimate (3) is the nonexistence of unconditional mean squared error (MSE, i.e., the expected squared \mathcal{L}^2 discrepancy), as the denominator in (3) is zero with a positive probability for finite sample. This can be overcome by ridging, as used by Fan (1993) and discussed

in more details by Seifert and Gasser (1996) and Hall and Marron (1997). We thus use a ridged local linear estimate for $X_i(t)$

$$\hat{X}_i(t) = \frac{R_0 S_2 - R_1 S_1}{S_0 S_2 - S_1^2 + \delta 1_{\{|S_0 S_2 - S_1^2| < \delta\}}}, \quad (4)$$

where $\delta > 0$ is a sufficiently small constant depending on m_i , e.g., a convenient choice is $\delta = m_i^{-2}$.

To characterize the manifold structure in FREM, we estimate the tangent space at the given x explicitly and then perform local linear smoothing on the coordinates $\hat{\mathbf{x}}_i$ of the observations \hat{X}_i when projected onto the estimated tangent space. To do so, we shall first determine the intrinsic dimension d of the manifold \mathcal{M} . We adopt the maximum likelihood estimator proposed by Levina and Bickel (2004), substituting the unobservable X_i with the contaminated version \hat{X}_i . Denoting $\hat{G}_i(x) = \|x - \hat{X}_i\|_{\mathcal{L}^2}$ and $\hat{G}_{(k)}(x)$ the k th order statistic of $\hat{G}_1(x), \dots, \hat{G}_n(x)$, then

$$\hat{d} = \frac{1}{k_2 - k_1 + 1} \sum_{k=k_1}^{k_2} \hat{d}_k, \quad \text{with } \hat{d}_k = \frac{1}{n} \sum_{i=1}^n \hat{d}_k(\hat{X}_i), \quad \hat{d}_k(x) = \left\{ \frac{1}{k-1} \sum_{j=1}^{k-1} \log \frac{\hat{G}_{(k)}(x) + \Delta}{\hat{G}_{(j)}(x) + \Delta} \right\}^{-1}, \quad (5)$$

where Δ is a positive constant depending on n , and k_1 and k_2 are tuning parameters. Note that, in order to overcome the additional variability introduced by contamination, we regularize $\hat{d}_k(x)$ by an extra term Δ . We conveniently set $\Delta = 1/\log n$, while refer readers to Levina and Bickel (2004) for the choice of k_1 and k_2 . Given the estimate \hat{d} , we proceed to estimate the tangent space at the given point x as follows.

- A neighborhood of x is determined by a tuning parameter $h_{pca} > 0$, denoted by $\hat{\mathcal{N}}_{\mathcal{L}^2}(h_{pca}, x) = \{\hat{X}_i : \|x - \hat{X}_i\|_{\mathcal{L}^2} < h_{pca}, i = 1, 2, \dots, n\}$.
- Compute the local empirical covariance function

$$\hat{\mathcal{C}}_x(s, t) = \frac{1}{|\hat{\mathcal{N}}_{\mathcal{L}^2}(h_{pca}, x)|} \sum_{\hat{X} \in \hat{\mathcal{N}}_{\mathcal{L}^2}(h_{pca}, x)} \{\hat{X}(s) - \hat{\mu}_x(s)\} \{\hat{X}(t) - \hat{\mu}_x(t)\} \quad (6)$$

using the data within $\hat{\mathcal{N}}_{\mathcal{L}^2}(h_{pca}, x)$ and obtain eigenvalues $\hat{\rho}_1 > \hat{\rho}_2 > \dots > \hat{\rho}_{\hat{d}}$ and corresponding eigenfunctions $\hat{\varphi}_1, \hat{\varphi}_2, \dots, \hat{\varphi}_{\hat{d}}$, where $\hat{\mu}_x = |\hat{\mathcal{N}}_{\mathcal{L}^2}(h_{pca}, x)|^{-1} \sum_{\hat{X} \in \hat{\mathcal{N}}_{\mathcal{L}^2}(h_{pca}, x)} \hat{X}$ is the local mean function and $|\hat{\mathcal{N}}_{\mathcal{L}^2}(h_{pca}, x)|$ denotes the number of observations in $\hat{\mathcal{N}}_{\mathcal{L}^2}(h_{pca}, x)$. This can be done by standard functional principal component analysis (FPCA) procedures, such as Yao *et al.* (2005a) and Hall and Hosseini-Nasab (2006).

- Estimate the tangent space at x by $\widehat{T_x \mathcal{M}} = \text{span}\{\hat{\varphi}_1, \hat{\varphi}_2, \dots, \hat{\varphi}_{\hat{d}}\}$, the linear space spanned by the first \hat{d} eigenfunctions.

Note that the eigen-decomposition of the function $\hat{\mathcal{C}}_x(s, t)$ provides a local Karhunen-Loëve expansion of X at the given x which is used to construct an estimate of the tangent space at x . Finally, we project all \hat{X}_i onto the estimated tangent space $\widehat{T_x \mathcal{M}}$ and obtain coordinates $\hat{\mathbf{x}}_i = (\langle \hat{X}_i, \hat{\varphi}_1 \rangle, \dots, \langle \hat{X}_i, \hat{\varphi}_{\hat{d}} \rangle)^T$. Then, the estimate of $g(x)$ is given by

$$\hat{g}(x) = \mathbf{e}_1^T (\hat{\mathbf{X}}^T \hat{\mathbf{W}} \hat{\mathbf{X}})^{-1} \hat{\mathbf{X}}^T \hat{\mathbf{W}} \mathbf{Y}, \quad \text{where} \quad \hat{\mathbf{X}} = \begin{pmatrix} 1 & 1 & \dots & 1 \\ \hat{\mathbf{x}}_1 & \hat{\mathbf{x}}_2 & \dots & \hat{\mathbf{x}}_n \end{pmatrix}^T, \quad (7)$$

$\hat{\mathbf{W}} = \text{diag}(K_{h_{reg}}(\|x - \hat{X}_1\|_{\mathcal{L}^2}), K_{h_{reg}}(\|x - \hat{X}_2\|_{\mathcal{L}^2}), \dots, K_{h_{reg}}(\|x - \hat{X}_n\|_{\mathcal{L}^2}))$ with $K_h(t) = K(t/h)/h^{\hat{d}}$ and the bandwidth h_{reg} , $\mathbf{Y} = (Y_1, Y_2, \dots, Y_n)^T$, and $\mathbf{e}_1^T = (1, 0, 0, \dots, 0)$ is an $n \times 1$ vector. Note that the matrix $\hat{\mathbf{X}}$ incorporates the estimated geometric structure that is encoded by the local eigenbasis $\hat{\varphi}_1, \dots, \hat{\varphi}_{\hat{d}}$. The tuning parameter h_{reg} , along with h_{pca} , is selected by modified generalized cross-validation detailed in Cheng and Wu (2013). We emphasize that, in the above estimation procedure which is illustrated by a diagram in the left panel of Figure 1, all steps are based on the contaminated sample $\{\hat{X}_1, \dots, \hat{X}_n\}$, rather than the unavailable functions X_i .

In practice, the predictor x is often not fully observed either. Instead, it is measured at m_x discrete points t_1, \dots, t_{m_x} , and the measurements are corrupted by random noise. In this case, we then estimate x by the same local linear smoothing method as in (2). We denote this estimate by \tilde{x} , and replace x with \tilde{x} in (5)–(7) to obtain an estimate of $g(\tilde{x})$.

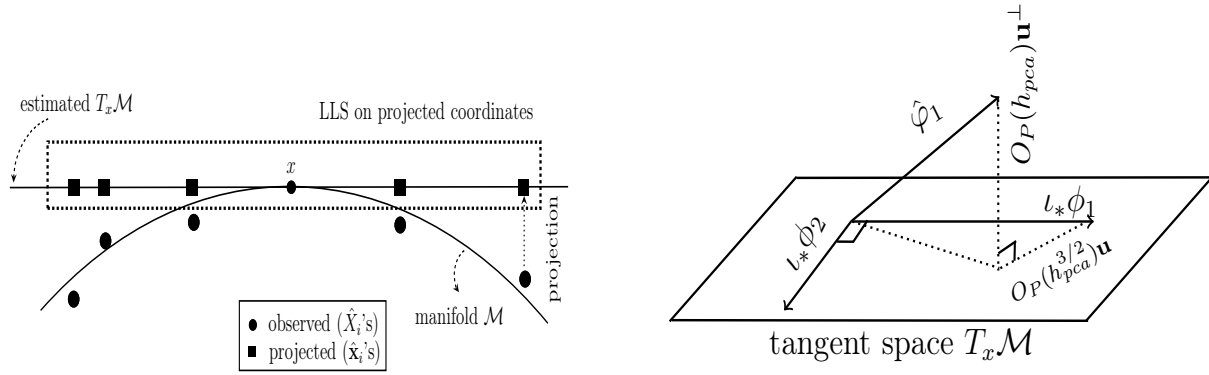


Figure 1: Left: illustration of functional regression on manifold; Right: illustration of estimation quality of the tangent space at x .

3 Theoretical Properties

In this section, we investigate the theoretical properties of the estimate $\hat{g}(x)$ in (7). Recalling that m_i denotes the number of measurements for the predictor X_i , we assume that m_i grows with sample size n at a polynomial rate. Without loss of generality, assume $m_i \asymp m \asymp n^\alpha$ for some constant $\alpha > 0$, where $a_n \asymp b_n$ denotes $0 < \liminf a_n/b_n < \limsup a_n/b_n < \infty$. The random noise ζ_{ij} is assumed to be i.i.d. for simplicity. It is worth pointing out that the development below can be modified to accommodate weakly dependent and heterogeneous noise. This generality will introduce considerably more tedious derivations without adding further insight, which is not pursued here. The discrepancy between \hat{X}_i and X_i , quantified by $\|\hat{X}_i - X_i\|_{\mathcal{L}^2}$, is termed *contamination* of X_i . It turns out that, the decay of this contamination is intimately linked to the consistency of the estimates of the intrinsic dimension, the tangent spaces, and eventually the regression functional $g(x)$. As one of our main contributions, we discover that the convergence rate of $\hat{g}(x)$ exhibits a phase transition phenomenon depending on the interplay between the intrinsic dimension and the decay of contamination. We start with the property of contamination in recovery of functional data to set the stage.

Recall that the individual smoothing to recover each X_i is based on the measurements available

for that individual, $\mathbb{X}_i = \{(T_{i1}, X_{i1}^*), (T_{i2}, X_{i2}^*), \dots, (T_{im}, X_{im}^*)\}$, so the estimates \hat{X}_i are also i.i.d. if the observed data are i.i.d., which simplifies our analysis and can be extended to weakly dependent \hat{X}_i without substantial changes. Specifically, we study the p th moment of contamination in \mathcal{L}^2 norm when \hat{X}_i is the ridged local linear estimate given by (4), while Fan (1993) derived the convergence rate of $\|\hat{X}_i - X_i\|_{\mathcal{L}^2}^2$ conditional on X_i , i.e., a special case of $p = 2$. As a matter of fact, our result below for an arbitrary p th moment is not present in the literature.

Let $\Sigma(\nu, L)$ denote the Hölder class with exponent ν and Hölder constant L , which represents the set of $\ell = \lfloor \nu \rfloor$ times differentiable functions F whose derivative $F^{(\ell)}$ satisfies $|F^{(\ell)}(t) - F^{(\ell)}(s)| \leq L|t - s|^{\nu - \ell}$ for $s, t \in D$, where $\lfloor \nu \rfloor$ is the largest integer strictly smaller than ν . We require mild assumptions as follows, and assume $h_i \asymp h_0$ without loss of generality.

(A1) K is a differentiable kernel with a bounded derivative, $\int_{-1}^1 K(u)du = 1$, $\int_{-1}^1 uK(u)du = 0$, and $\int_{-1}^1 |u|^p K(u)du < \infty$ for all $p > 0$.

(A2) The sampling density f_T is bounded away from zero and infinity, i.e., for some constants $C_{T,1}, C_{T,2} \in (0, \infty)$, $C_{T,1} = \inf_{t \in D} f_T(t) \leq \sup_{t \in D} f_T(t) = C_{T,2}$.

(A3) $X \in \Sigma(\nu, L_X)$, where $L_X > 0$ is a random quantity and $0 < \nu \leq 2$ is some constant that quantifies the smoothness of the process.

(A4) For all $r \geq 1$, $\mathbf{E} \sup_t |X(t)|^r < \infty$, $\mathbf{E}(L_X)^r < \infty$ and $\mathbf{E}|\zeta|^r < \infty$.

Note that $\mathbf{E} \sup_t |X(t)|^r < \infty$ holds rather generally, as discussed in Li and Hsing (2010); Zhang and Wang (2010) compared to a stronger assumption on X given in (A.1) of Hall *et al.* (2006). The following proposition is an immediate consequence of Lemma S.1 in the Supplementary Material, and hence its proof is omitted.

Proposition 1 *For any $p \geq 1$, assume $\mathbf{E}|\zeta|^p < \infty$. Under assumptions (A1)–(A3), for the estimate \hat{X} in (4) with $h_0 \asymp m^{-\frac{1}{2\nu+1}}$ and a proper choice of δ , we have*

$$\{\mathbf{E}(\|\hat{X} - X\|_{\mathcal{L}^2}^p \mid X)\}^{1/p} = O(m^{-\frac{\nu}{2\nu+1}}) \left\{ \sup_t |X(t)| + L_X \right\}. \quad (8)$$

Furthermore, if additionally assumption (A4) holds and $m \asymp n^\alpha$ for some $\alpha > 0$, then

$$\left(\mathbf{E} \|\hat{X} - X\|_{\mathcal{L}^2}^p \right)^{1/p} = O(n^{-\frac{\alpha\nu}{2\nu+1}}).$$

When X is deterministic as in nonparametric regression, the rate in (8) for $p = 2$ coincides with that in Tsybakov (2008). Note that the p th order of the contamination $\|\hat{X}_i - X_i\|_{\mathcal{L}^2}$ decays at a polynomial rate which depends on the sampling rate α and smoothness ν , but not the order of p .

Now we begin derivation of the asymptotic property of the estimator \hat{g} . Recall that \mathcal{M} is assumed to be embedded in $\mathcal{L}^2(D)$ in model (1). Since both the manifold \mathcal{M} and the associated isometric embedding, denoted by ι , are hidden and only observable through $\iota(\mathcal{M})$ in the ambient space $\mathcal{L}^2(D)$, we can equivalently treat the manifold \mathcal{M} as an unknown finite-dimensional submanifold of $\mathcal{L}^2(D)$, and accordingly treat the embedding map ι as the inclusion map. Therefore, in the sequel, we shall use x and X to denote both $x, X \in \iota(\mathcal{M})$ and $\iota^{-1}(x), \iota^{-1}(X) \in \mathcal{M}$ when no ambiguity arises.

We shall point out that the isometric embedding of the manifold into $\mathcal{L}^2(D)$ is assumed to *a priori* exist. Similar setup has been commonly adopted in the literature such as, among many others, Tenenbaum *et al.* (2000) and Cheng and Wu (2013) with a finite-dimensional ambient space, and Chen and Müller (2012) with an infinite-dimensional ambient space. In our case, as the ambient space is the infinite-dimensional $\mathcal{L}^2(D)$ rather than the more familiar Euclidean spaces, one might be concerned of the mathematical plausibility of such assumption. To establish the plausibility, it is sufficient to exhibit one example of such embedding, or equivalently a finite-dimensional submanifold of $\mathcal{L}^2(D)$. In Example 1, we have constructed an isometric embedding of the unit circle into $\mathcal{L}^2(D)$, with the embedded image being a one-dimensional submanifold of $\mathcal{L}^2(D)$. In fact, uncountable number of examples of any dimension can be constructed in a similar fashion. This not only justifies the mathematical plausibility of our *a priori* manifold assumption, but also demonstrates the abundance of finite-dimensional submanifolds of $\mathcal{L}^2(D)$.

To analyze the asymptotic property of $\hat{g}(x)$, we make following assumptions.

(B1) The probability density f of X on \mathcal{M} satisfies $C_{f,1} = \inf_{x \in \mathcal{M}} f(x) \leq \sup_{x \in \mathcal{M}} f(x) = C_{f,2}$

for some constants $0 < C_{f,1} \leq C_{f,2} < \infty$.

(B2) The regression functional g is twice differentiable with a bounded second derivative.

(B3) $\hat{X}_1, \hat{X}_2, \dots, \hat{X}_n$ are independently and identically distributed. For some $\beta \in (0, \infty)$ and all $p \geq 1$, $\{\mathbf{E}(\|\hat{X} - X\|_{\mathcal{L}^2}^p \mid X)\}^{1/p} \leq C_p n^{-\beta} \eta(X)$ for some constant C_p depending only on p and some nonnegative function $\eta(X)$ depending only on X such that $\mathbf{E}\{\eta(X)\}^p < \infty$.

For (B1), since the predictor functions resides on a low-dimensional manifold, the existence of a density can be safely assumed. Note that the assumption (B3) is presented in terms of the contaminated predictor \hat{X} , and hence implicitly poses requirement for the smoothing method. Under assumptions (A1)–(A4), by Proposition 1, the individual smoothing via local linear estimation (4) satisfies (B3) with $\beta = \alpha\nu/(2\nu + 1)$. To give an intuitive interpretation, we define $\gamma = \beta^{-1} = (2 + \nu^{-1})/\alpha$ as the contamination level of \hat{X} . We see that the contamination level is low for densely observed (i.e., large α) or smoother (i.e., large ν) functions. We emphasize that our theory on the estimated regression functional \hat{g} does not depend on the smoothing method used in recovering X_i , as long as (B3) is fulfilled. Further, we may extend (B3) to allow weak independence and heterogeneous distribution of $\{\hat{X}_1, \dots, \hat{X}_n\}$ by modifying proofs. This will accommodate weakly dependent functional data or the contaminated \hat{X}_i that are attained by borrowing information across individuals (e.g. Yao *et al.*, 2005a), which is beyond our scope here and can be a topic of future research.

The contamination of the predictor X poses substantial challenge on the estimation of the manifold structures. For instance, the quality of the tangent space at x , denoted by $T_x\mathcal{M}$, crucially depends on a bona fide neighborhood around x , while the contaminated neighborhood $\hat{\mathcal{N}}_{\mathcal{L}^2}(h_{pca}, x)$ and the inaccessible true neighborhood $\mathcal{N}_{\mathcal{L}^2}(h_{pca}, x) = \{X_i : \|X_i - x\|_{\mathcal{L}^2} < h_{pca}\}$ might contain different observations. Fortunately we can show that they are not far apart in the sense of Proposition S.2 in the Supplementary Material. In practice, we suggest to choose $\max(h_{reg}, h_{pca}) < \min\{2/\tau, \text{inj}(\mathcal{M})\}/4$, where τ is the condition number of \mathcal{M} and $\text{inj}(\mathcal{M})$ is the injectivity radius of \mathcal{M} (Cheng and Wu, 2013), so that $\hat{\mathcal{N}}_{\mathcal{L}^2}(h_{pca}, x)$ provides a good approximation of the true neigh-

borhood of x within the manifold. The following result concerns the estimation quality of the local manifold structures, where $\iota_* T_x \mathcal{M}$ represents the embedded tangent space at $\iota(x)$, with ι_* denoting the differential of the embedding ι .

Theorem 1 *Under assumptions (B1) and (B3), we have*

1. \hat{d} is a consistent estimator of d when $\min\{k_1, k_2\} \rightarrow \infty$ and $\max\{k_1, k_2\}/n \rightarrow 0$.
2. Let $\varrho = 1/(d+2)$ if $\beta \geq 2/d$ and $\varrho = \beta/2$ otherwise, $h_{pca} \asymp n^{-\varrho}$. Then the eigenbasis $\{\hat{\varphi}_k\}_{k=1}^d$ derived from $\hat{\mathcal{C}}_x$ in (6) is close to an orthonormal basis $\{\phi_k\}_{k=1}^d$ of $T_x \mathcal{M}$: if $x \in \mathcal{M}$, for $k = 1, 2, \dots, d$,

$$\hat{\varphi}_k = \iota_* \phi_k + O_P(h_{pca}^{3/2}) \mathbf{u}_k + O_P(h_{pca}) \mathbf{u}_k^\perp, \quad (9)$$

where $\mathbf{u}_k \in \iota_* T_x \mathcal{M}$, $\mathbf{u}_k^\perp \perp \iota_* T_x \mathcal{M}$, and $\|\mathbf{u}_k\|_{\mathcal{L}^2} = \|\mathbf{u}_k^\perp\|_{\mathcal{L}^2} = 1$.

In light of Theorem 1.1, we shall from now on present the subsequent results by conditioning on the event $\hat{d} = d$, and the right panel of Figure 1 provides a geometric illustration of equation (9) for the case $d = 2$. Note that, although the curvature at x does not appear in the asymptotic rates in (9), it does play a role as a constant that is absorbed into the O_P terms. The intuition is that, no matter how large the curvature is at x , as long as it is fixed and bounded away from infinity, the \mathcal{L}^2 distance can serve as a good approximation to the metric (distance) of objects on the manifold \mathcal{M} , provided that the distance of these objects is sufficiently small; e.g., Lemma A.2.3 of Cheng and Wu (2013). In practice, it is usually more difficult to estimate the tangent structure at a point with larger curvature.

We are ready to state the results on the estimated regression functional. Recall that $\hat{g}(x)$ in (7) is obtained by applying local linear smoother on the coordinates of contaminated predictors within the estimated tangent space at x . It is well known that local linear estimator does not suffer from boundary effects, i.e., the first order behavior of the estimator at the boundary is the same as in the interior (Fan, 1992). However, the contamination on predictor has different impact, and we shall address the interior and boundary cases separately. Denote $\mathcal{X} = \{(X_1, \hat{X}_1), (X_2, \hat{X}_2), \dots, (X_n, \hat{X}_n)\}$

and $\mathcal{M}_h = \{x \in \mathcal{M} : \inf_{y \in \partial\mathcal{M}} \mathfrak{d}(x, y) \leq h\}$, where $\partial\mathcal{M}$ denotes the boundary of \mathcal{M} and $\mathfrak{d}(\cdot, \cdot)$ denotes the distance function on \mathcal{M} . For points sufficiently far away from the boundary of \mathcal{M} , we have the following result about the conditional mean square errors (MSE) of the estimate $\hat{g}(x)$.

Theorem 2 *Assume that (A1) and (B1)–(B3) hold. Let $x \in \mathcal{M} \setminus \mathcal{M}_{h_{reg}}$ and h_{pca} chosen as in Theorem 1(2). For any $\epsilon > 0$, if we choose $h_{reg} \asymp n^{-1/(d+4)}$ when $\beta > 3/(d+4)$, and $h_{reg} \asymp n^{-\beta/(3+\epsilon d)}$ when $\beta \leq 3/(d+4)$, then*

$$\mathbf{E} [\{\hat{g}(x) - g(x)\}^2 \mid \mathcal{X}] = O_P \left(n^{-\frac{4}{d+4}} + n^{-\frac{4\beta}{3+\epsilon d}} \right). \quad (10)$$

We emphasize the following observations from this theorem. First, the convergence rate of $\hat{g}(x)$ is a polynomial of the sample size n depending on both the intrinsic dimension d and the *contamination level* defined as $\gamma = \beta^{-1}$. This is in contrast with traditional functional nonparametric regression methods that do not explore the intrinsic structure, which cannot reach a polynomial rate of convergence. Second, when contamination level $\gamma < \gamma_0 = (d+4)/3$, the intrinsic dimension dominates the convergence rate in (10), while when $\gamma \geq \gamma_0$, the contamination dominates. Thus the convergence rate exhibits a phase transition separated at the threshold level γ_0 . Intuitively, when the contamination is low, the manifold structure can be estimated reliably and hence determines the quality of the estimated regression. On the other hand, when the contamination passes the threshold γ_0 , the manifold structure is buried by noise and cannot be well utilized. Third, it is observed that the phase transition threshold γ_0 increases with the intrinsic dimension d that indicates the complexity of a manifold. This interesting finding suggests that, although estimating a complex manifold is more challenging (i.e., slower rate), such a manifold is more resistant to contamination.

Theorem 2 can be also interpreted by relating the sampling rate m and the sample size n . Recall that $m \geq n^\alpha$ and $\gamma = (2 + \nu^{-1})/\alpha$, where ν denotes the Hölder smoothness of the process X as in (A3). When the sampling rate is low, $\alpha \leq 3(2 + \nu^{-1})/(d+4)$, i.e., $m \lesssim n^{3(2+\nu^{-1})/(d+4)}$, the contamination reflected by the second term in the right hand side (r.h.s.) of (10) dominates and is actually determined by m . Otherwise the first term prevails and involves only the sample size n and

the intrinsic dimension prevails. In the literature of functional data analysis, ν is typically at least 2, i.e., continuously twice differentiable. For a moderate dimension such as $d = 6$, the contamination blurs the estimation of g when $m \lesssim n^{3/4}$, and becomes asymptotically negligible otherwise, where $a_n \lesssim b_n$ denotes $a_n/b_n \rightarrow 0$.

The above interpretation clearly separates our theory from that in Cheng and Wu (2013) where the actual observed predictor comes from a finite and fixed dimensional Euclidean space without noise. In the functional setup, actual observed predictor is $\mathbb{X}_i = \{(T_{i1}, X_{i1}^*), (T_{i2}, X_{i2}^*), \dots, (T_{im}, X_{im}^*)\}$ (under assumption $m_i \equiv m$), which is an m -dimensional vector whose distribution is *fully* supported on \mathbb{R}^m due to the presence of noise ζ_{ij} , rather than a low-dimensional subspace of \mathbb{R}^m . This implies that the support of the distribution of \hat{X}_i is also m -dimensional. The smoothness structure of functional data could help tighten the distribution of \hat{X}_i , but does not reduce its dimension. Thus, as m goes to infinity, it might raise a serious concern of curse of dimensionality. In this sense, the polynomial rate and phase transition phenomenon in Theorem 2 is nontrivial: when m is small relative to the sample size n , it determines the convergence rate, while when it surpasses certain threshold, by explicitly exploring the low-dimensional manifold structure, the growing dimension of the contamination can be defeated with the aid of smoothness, so that m does not play a role any more in the convergence rate. Next theorem characterizes the asymptotic behavior of \hat{g} at x close to the boundary of \mathcal{M} .

Theorem 3 *Assume that (A1) and (B1)–(B3) hold. Let $x \in \mathcal{M}_{h_{reg}}$ and h_{pca} chosen as in Theorem 1. For any $\epsilon > 0$, if we choose $h_{reg} \asymp n^{-1/(d+4)}$ when $\beta > 4/(d+4)$, and $h_{reg} \asymp n^{-\beta/(4+\epsilon d)}$ when $\beta \leq 4/(d+4)$, then the conditional MSE satisfies*

$$\mathbf{E} [\{\hat{g}(x) - g(x)\}^2 \mid \mathcal{X}] = O_P \left(n^{-\frac{4}{d+4}} + n^{-\frac{4\beta}{4+\epsilon}} \right). \quad (11)$$

It is interesting to note that the effect of the intrinsic dimension on convergence is the same, regardless where \hat{g} is evaluated on the manifold. However, the effect of contamination behaves differently, due to the fact that the second order behavior of local linear estimator that depends

on the location needs to be taken into account when there is contamination on X . We see that when contamination effect dominates, the convergence is slightly slower for boundary points than for interior points, and the phase transition occurs at $\gamma_0 = (d + 4)/4$. This is the price we pay for the boundary effect when predictors are contaminated, which is in contrast with the classical result on local linear estimator (Fan, 1993).

Finally, we address the case that the predictor x is not fully observed. It is reasonable to assume that x comes from the same source of the data, in the sense that its smoothed version \tilde{x} has the same contamination level as those $\hat{X}_1, \dots, \hat{X}_n$, as per (B3). To be specific, assume that

$$(B4) \quad \text{the estimate } \tilde{x} \text{ is independent of } X_1, \dots, X_n \text{ and } \mathbb{X}_1, \dots, \mathbb{X}_n. \text{ Also } \{\mathbf{E}\|\tilde{x} - x\|_{\mathcal{L}^2}^p\}^{1/p} \leq C'_p n^{-\beta} \text{ for all } p \geq 1, \text{ where } C'_p \text{ is constant depending on } p \text{ only.}$$

Note that the independent condition in (B4) is satisfied if t_1, \dots, t_{m_x} are independent of X_1, \dots, X_n and $\mathbb{X}_1, \dots, \mathbb{X}_n$. The second part of (B4) is met if assumptions similar to (A1)-(A4) hold also for x and t_1, \dots, t_{m_x} , according to Proposition 1.

Theorem 4 *With conditions (A1), (B1)-(B3), and additional assumption (B4), equation (10) holds when $x \in \mathcal{M} \setminus \mathcal{M}_{h_{reg}}$, and equation (11) holds when $x \in \mathcal{M}_{h_{reg}}$, both with $\hat{g}(x)$ replaced by $\hat{g}(\tilde{x})$.*

4 Simulation Study

To demonstrate the performance of our FREM framework, we conduct simulations for three different manifold structures, namely, the three-dimensional rotation group $SO(3)$, the Klein bottle (Klein) and the mixture of two Gaussian densities (MixG). For all settings, a functional predictor X_i is observed at $m = 100$ equally spaced points T_1, T_2, \dots, T_m in the interval $[0, 1]$ with heteroscedastic measurement error $\epsilon_{ij} \sim N(0, \sigma_j^2)$, where σ_j is determined by the signal-to-noise ratio on $X(T_j)$ so that $\text{snrdb}_X = \text{Var}\{X(T_j)\}/\sigma_j^2 = 4$. The response is generated by $Y_i = 4 \sin(4Z_i) \cos(Z_i^2) + 2\Gamma(1 + Z_i/2) + \varepsilon_i$ with $Z_i = \int_0^1 X_i^2(t) dt$ and $\Gamma(\alpha) = \int_0^\infty s^{\alpha-1} e^{-s} ds$ the gamma function. The noise ε_i on response Y is a centered Gaussian variable with variance σ_ε^2 that is determined by the signal-to-noise ratio on Y so that $\text{snrdb}_Y = \text{Var}(Y)/\sigma_\varepsilon^2 = 2$. Other information of each setting is provided below.

- **SO(3):** $X_i(t) = \sum_{k=1}^9 \xi_{ik} b_k(t)$, where $\phi_{2\ell-1}(t) = \cos\{(2\ell-1)\pi t/10\}/\sqrt{5}$ and $\phi_{2\ell}(t) = \sin\{(2\ell-1)\pi t/10\}/\sqrt{5}$. To generate random variables ξ_{ik} , we define vector $\mathbf{r} = (r_1, r_2, r_3)$ and matrix

$$\mathbf{R}(\mathbf{r}, \theta) = (1 - \cos \theta) \mathbf{r} \mathbf{r}^T + \begin{pmatrix} \cos \theta & -r_3 \sin \theta & r_2 \sin \theta \\ r_3 \sin \theta & \cos \theta & -r_1 \sin \theta \\ -r_2 \sin \theta & r_1 \sin \theta & \cos \theta \end{pmatrix}.$$

Denote $\mathbf{e}_2 = (1, 0, 0)^T$ and similarly \mathbf{e}_3 , and we generate $(\xi_{i1}, \dots, \xi_{i9})^T = \text{vec}(\mathbf{Z}_i)$ with

$$\mathbf{Z}_i = \mathbf{R}(\mathbf{e}_3, u_i) \mathbf{R}(\mathbf{e}_2, v_i) \mathbf{R}(\mathbf{e}_3, w_i), \quad (12)$$

where (u_i, v_i) are i.i.d. random pairs uniformly distributed on the 2D sphere $S^2 = [0, 2\pi) \times [0, \pi]$, and w_i are i.i.d. uniformly distributed on the unit circle $S^1 = [0, 2\pi)$. Note that (12) is the Euler angles parameterization of $SO(3)$ (Stuelpnagel, 1964) that has an intrinsic dimension $d = 3$.

- **Klein:** $X_i(t) = \sum_{k=1}^4 \xi_{ik} \phi_k(t)$ with ϕ_k as in the $SO(3)$ setting. For random variables ξ_k , we use $\xi_{i1} = (2 \cos v_i + 1) \cos u_i$, $\xi_{i2} = (2 \cos v_i + 1) \sin u_i$, $\xi_{i3} = 2 \sin v_i \cos(u_i/2)$ and $\xi_{i4} = 2 \sin v_i \sin(u_i/2)$, where $u_i, v_i \stackrel{i.i.d.}{\sim} \text{Unif}(0, 2\pi)$. Here $(u, v) \mapsto (\xi_1, \xi_2, \xi_3, \xi_4)$ is a parametrization of Klein bottle with an intrinsic dimension $d = 2$.
- **MixG:** X_i is a mixture of two Gaussian densities, i.e., $X_i(t) = \exp\{-(t - u_i)^2/2\}/\sqrt{2\pi} + \exp\{-(t - v_i)^2/2\}/\sqrt{2\pi}$ with $(v_1, v_2)^T$ uniformly sampled from a circle with diameter 0.5, similar to that used in Chen and Müller (2012).

Note that, to see the impact of manifold structures on regression, we normalize the functional predictor in all settings to the unit scale, i.e, multiplying X by the constant $c = 1/\sqrt{\mathbf{E}\|X\|^2}$ so that the resultant X satisfies $\mathbf{E}\|X\|^2 = 1$. Such scaling does not change the geometric structure of manifolds but the size. In order to account for at least 95% of variance of the contaminated data, we find empirically that more than 10 principal components are needed in all settings, i.e.,

the dimensions of the contaminated data are considerably larger than their intrinsic dimensions.

For each setting, three different sample sizes are considered, $n = 250$, $n = 500$ and $n = 1000$. For evaluation, we generate independent test data of size 5000, and compute the square-root of mean square error (rMSE) using the test data. It is noted that in the test data, each predictor is also discretely measured and contaminated by noise in the same way of the training sample. For comparison, we compute the rMSE for various functional nonparametric regression methods described in Ferraty and Vieu (2006): functional Nadaraya-Watson estimator (FNW), functional conditional expectation (FCE), functional mode (FMO), functional conditional median (FCM) and the multi-method (MUL) that averages estimates from FCE, FMO and FCM. Functional linear regression (FLR) is also included to illustrate the impact of nonlinear relationship not captured by FLR. The tuning parameters in these methods, such as the number of principal components for FLR and the bandwidth for FNW, FCE, FMO and FCM, are selected by 10-fold cross validation. We repeat each study 100 times independently, and the results are presented in Table 4.

First, we observe that FREM enjoys favorable numerical performance in all simulation settings. Second, as sample size grows, the reduction in rMSE is more prominent for FREM than for the other methods. Take FNW and FREM in the Klein setting for example. The relative rMSE reduction from $n = 250$ ($n = 500$, respectively) to $n = 500$ ($n = 1000$, respectively) is 25.5% (22.7%, respectively) for FREM, and 8.49% (2.75%, respectively) for FNW. This may provide some numerical evidence that the proposed FREM has a faster convergence rate compared to its counterparts (Mas, 2012). Furthermore, it also provides evidence for the polynomial rate stated in Theorem 2–4, based on which the relative reduction is expected to be $1 - (n_1/n_2)^{2/(d+4)}$ with sample size from n_1 to n_2 . For Klein setting, it is about 20.6%, and the empirical relative reduction is 22.7% from $n_1 = 500$ to $n_2 = 1000$. Similar observations can be made for other settings. In contrast, the existing kernel methods perform no better than a logarithmic rate, providing numerical evidence for the theory of Mas (2012). Take FNW as example. The empirical relative reduction is 2.75% from $n_1 = 500$ to $n_2 = 1000$, even less than what the logarithmic rate suggests, $1 - \log(500)/\log(1000) \approx 10.0\%$. Third, as the intrinsic dimension goes up, the relative rMSE

Table 1: Shown are the Monte Carlo averages of square-root mean square error (rMSE) and its standard error in parenthesis based on 100 independent simulation runs, for different settings and methods described in Section 4, in the scale of 10^{-1} .

	SO(3)			Klein Bottle			MixG		
	$n = 250$	$n = 500$	$n = 1000$	$n = 250$	$n = 500$	$n = 1000$	$n = 250$	$n = 500$	$n = 1000$
FLR	2.21(.034)	2.18(.023)	2.16(.020)	6.13(.062)	6.12(.039)	6.09(.035)	2.96(.143)	2.90(.126)	2.88(.099)
FNW	1.62(.058)	1.57(.043)	1.55(.032)	3.18(.405)	2.91(.179)	2.83(.068)	1.87(.146)	1.75(.083)	1.70(.065)
FCE	1.53(.066)	1.41(.052)	1.32(.030)	2.97(.146)	2.71(.104)	2.61(.081)	2.11(.132)	2.04(.093)	1.98(.064)
FMO	2.54(.116)	2.30(.094)	2.20(.085)	4.62(.307)	4.12(.220)	3.83(.187)	3.59(.280)	3.36(.205)	3.22(.161)
FCM	2.02(.060)	1.86(.052)	1.72(.035)	3.91(.267)	3.39(.161)	3.09(.102)	2.73(.171)	2.51(.105)	2.32(.083)
MUL	1.82(.059)	1.66(.048)	1.54(.031)	3.40(.213)	3.00(.124)	2.77(.092)	2.46(.149)	2.31(.107)	2.18(.081)
FREM	1.01(.072)	.816(.056)	.638(.025)	1.65(.139)	1.23(.111)	.951(.074)	1.05(.132)	.808(.086)	.612(.075)

Table 2: Shown are the relative reduction of rMSE in percentage.

	SO(3)		Klein Bottle		MixG	
	$250 \rightarrow 500$	$500 \rightarrow 1000$	$250 \rightarrow 500$	$500 \rightarrow 1000$	$250 \rightarrow 500$	$500 \rightarrow 1000$
FLR	1.36	.917	.163	.490	2.02	.690
FNW	3.09	1.27	8.49	2.75	6.42	2.86
FCE	7.84	6.38	8.75	3.69	3.32	2.94
FMO	9.45	4.35	10.8	7.04	6.41	4.17
FCM	7.92	7.53	13.3	8.85	8.06	7.57
MUL	8.79	7.23	11.8	7.67	6.10	5.63
FREM	19.2	21.8	25.5	22.7	23.0	24.3

reduction for FREM decreases, suggesting that the intrinsic dimension plays an important role in convergence rate. Finally, different manifold structures result in different constants hidden in the O_P terms in Theorem 2 and 3, e.g., those in the $SO(3)$ setting are relatively smaller than their counterparts in the Klein setting, which agrees with the empirical results.

5 Real Data Examples

We apply FREM to analyze two real datasets. For the purpose of evaluation, we train our method on 75% of each dataset and reserve the other 25% as test data. The rMSE is computed on the

held-out test data. For comparison, we also compute rMSE for FLR, FNW, FCE, FMO and FCM as described in Section 4. We repeat this 100 times based on random partitions of the datasets, and present the Monte Carlo averages of rMSE together with their standard errors in Table 3.

The first application is to predict fat content of a piece of meat based on a spectrometric curve of spectra of absorbances for the meat using the Tecator dataset with 215 meat samples (Ferraty and Vieu, 2006). For each sample, the spectrometric curve for a piece of finely chopped pure meat was measured at 100 different wavelengths from 850 to 1050nm. Along with spectrometric curves, the fat content for each piece of meat was recorded. Comparing to the analytic chemistry required for measuring the fat content, obtaining a spectrometric curve is less time and cost consuming. As in Ferraty and Vieu (2006), we predict the fat content based on the first derivative curves approximated by the difference quotient between measurements at adjacent wavelengths, shown in the left panel of Figure 2. It is seen that there are some striking patterns around the middle wavelengths. The proposed FREM is able to capture these patterns by a low-dimensional manifold structure and yields more efficient estimates of fat content. For example, the FLR model uses 15.7 principal components on average with standard error 1.07, while the intrinsic dimension estimated by FREM is 5.05 with a standard error 0.62. From Table 3, FREM predicts the fat content more accurately than the other methods by a significant margin.

The second example studies the relationship between cognitive function and brain microstructure in the corpus callosum of patients with multiple sclerosis (MS), a common demyelinating disease caused by inflammation in the brain. It is observed that nerve cells are often covered by myelin, an insulating material that protects axons and helps nerve signal to travel faster. Demyelination refers to damage to myelin, which can result from immune-mediated inflammation, among other causes. Demyelination occurring in the white matter of brain, from which MS patients suffer, can potentially lead to loss of mobility or even cognitive impairment (Jongen *et al.*, 2012). Diffusion tensor imaging (DTI), a technique that can produce high-resolution images of white matter tissues by tracing water diffusion within the tissues, is an important method to examine potential myelin damage in the brain. For example, from the DTI images, some properties of white matter, such as

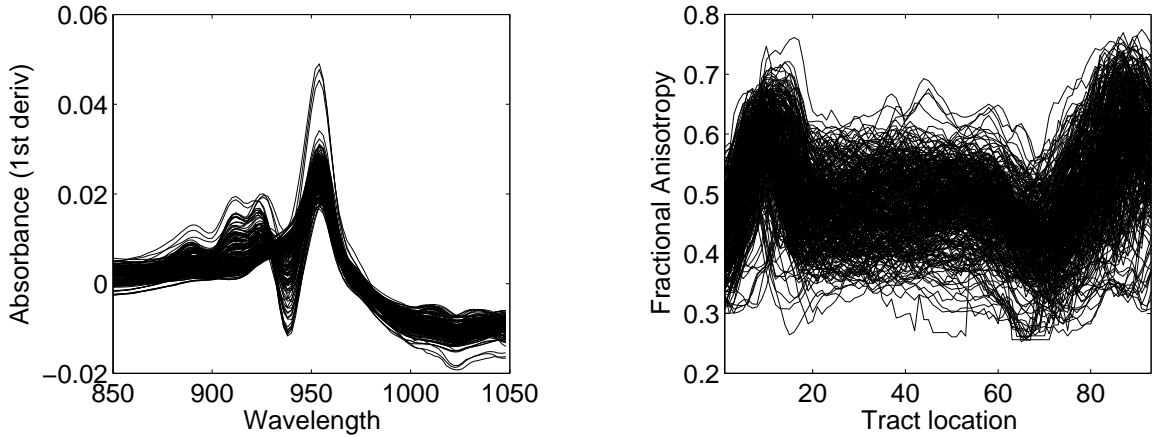


Figure 2: Left: first derivative curves of the spectra of absorbance for finely chopped 215 pure meat samples. Right: 340 fractional anisotropy profiles along corpus callosum tract location.

fractional anisotropy (FA) of water diffusion, can be derived. It has been shown that FA is related to multiple sclerosis (Ibrahim *et al.*, 2011).

To predict cognitive performance based on FA profiles for MS patients, we utilize the DTI data collected at Johns Hopkins University and the Kennedy-Krieger Institute. The data contains $n = 340$ FA profiles from MS patients and Paced Auditory Serial Addition Test (PASAT) scores that quantify cognitive function (Gronwall, 1977), where each FA profile is recorded at a grid of 93 points. In the right panel of Figure 2, we show all FA profiles, and observe that the data is considerably more complex than the spectrometric data. The average of estimated intrinsic dimensions is 5.82 with standard error 0.098. By contrast, the average number of principal components for FLR is 11.98 with standard error 5.22. According to Table 3, our method enjoys the most accurate prediction, followed by the FLR, while all other functional nonparametric methods deteriorate substantially.

SUPPLEMENTARY MATERIAL

Auxiliary results and technical lemmas with proofs, as well as the proof of Theorem 3 (similar to the proof of Theorem 2) are collected in an online Supplementary Material for space economy.

ACKNOWLEDGMENTS

Table 3: Shown are the Monte Carlo averages of square-root mean square error (rMSE) and its standard error based on 100 random partitions, for different methods on the meat spectrometric data and DTI data, where the results for DTI data is multiplied by 0.1 for visualization.

	FLR	FNW	FCE	FMO	FCM	MUL	FREM
Meat	2.56(.433)	2.42(.334)	1.97(.354)	2.66(.459)	2.82(.454)	2.31(.354)	1.06(.344)
DTI	1.14(.092)	1.28(.115)	1.36(.126)	1.78(.158)	1.25(.141)	1.33(.126)	.961(.089)

This research is partially supported by Natural Science and Engineering Research Council of Canada.

APPENDIX: EXAMPLE AND PROOFS OF THEOREMS

For illustration purpose, we present below a one-dimensional manifold embedded in $\mathcal{L}^2([0, 1])$ and a random process taking value in this manifold while having an infinite number of components in its Karhunen-Loëve expansion. Note that examples for dimensions larger than one can be constructed in a similar fashion.

Example 1 Let $S^1 = \{v_\omega = (\cos \omega, \sin \omega) : \omega \in [0, 2\pi)\}$ denote the unit circle regarded as a one-dimensional Riemannian manifold. Let $D = [0, 1]$ and denote ϕ_1, ϕ_2, \dots a complete orthonormal basis of $\mathcal{L}^2(D)$. Define map $X(v_\omega) = \sqrt{C} \sum_k k^{-c} \{\cos(k\omega)\phi_{2k-1} + \sin(k\omega)\phi_{2k}\}$ with $c > 3/2$ and $C = 1/\sum_k k^{-2c+2} \in (0, \infty)$. According to Proposition S.1 in Supplementary Material, X is an isometric embedding of S^1 into $\mathcal{L}^2(D)$. Moreover, no finite-dimensional linear subspace of $\mathcal{L}^2(D)$ fully encompasses the embedded image $X(S^1)$. A consequence of this observation is that, a random process taking samples from $X(S^1)$ might have an infinite number of eigenfunctions, even though $X(S^1)$ is merely one-dimensional, as we shall exhibit in the following. Let us treat S^1 as a probability space endowed with the uniform probability measure, and define random variables $\xi_{2k-1}(v_\omega) = \sqrt{C}k^{-c} \cos(k\omega)$ and $\xi_{2k}(v_\omega) = \sqrt{C}k^{-c} \sin(k\omega)$. Then $X = \sum_k \xi_k \phi_k$ can be regarded as a random process with samples from $X(S^1)$. It is easy to check that $\mathbf{E}(\xi_k \xi_j) = 0$ if $k \neq j$, $\mathbf{E}(\xi_k) = 0$, and $\mathbf{E}\xi_{2k-1}^2 = \mathbf{E}\xi_{2k}^2 = C\pi k^{-2c}$, which implies that $\mathbf{E}(\|X\|_{\mathcal{L}^2}^2) < \infty$. One can see that the eigenfunctions of the covariance operator of X are exactly ϕ_k . Therefore, $X = \sum_k \xi_k \phi_k$ is the

Karhunen-Loève expansion of the random process X , which clearly includes an infinite number of principal components, while X is intrinsically driven by the one-dimensional nonlinear manifold S^1 .

Below we shall provide proofs for Theorem 1 and 2, while the proof of Theorem 3 using similar techniques is deferred to the Supplementary Material. To reduce notational burden, $\mathcal{L}^2(D)$ is simplified by \mathcal{L}^2 , and we shall use $\|\cdot\|$ to denote the norm $\|\cdot\|_{\mathcal{L}^2}$ when no confusion arises.

PROOF OF THEOREM 1. (1) Without loss of generality, assume $x = 0$. Let $\tilde{G}_j = \hat{G}_j + \Delta$ and $\tilde{G}_{(1)}, \tilde{G}_{(2)}, \dots, \tilde{G}_{(k)}$ be the associated order statistics of $\tilde{G}_1, \tilde{G}_2, \dots, \tilde{G}_k$. Then,

$$\begin{aligned} & \left| \frac{1}{k-1} \sum_{j=1}^{k-1} \log \frac{\hat{G}_{(k)} + \Delta}{\hat{G}_{(j)} + \Delta} - \frac{1}{k-1} \sum_{j=1}^{k-1} \log \frac{G_{(k)}}{G_{(j)}} \right| \\ & \leq \left| \log \tilde{G}_{(k)} - \log G_{(k)} \right| + \left| \frac{1}{k-1} \sum_{j=1}^k \left(\log \tilde{G}_{(j)} - \log G_{(j)} \right) \right| \equiv I_1 + I_2. \end{aligned} \quad (13)$$

For I_1 , let q and q be the indices such that $\tilde{G}_{(k)} = \hat{G}_q$ and $G_{(k)} = G_q$, respectively. For the case $q = p$, we have $|\tilde{G}_{(k)} - G_{(k)}| = |\tilde{G}_p - G_p| \leq \left| \|\hat{X}_p\| - \|X_p\| \right| + \Delta \leq \|\hat{X}_p - X_p\| + \Delta$ by reverse triangle inequality. When $q \neq p$, it is seen that $\tilde{G}_p < \tilde{G}_{(k)} = \hat{G}_q$ and $G_q < G_p = G_{(k)}$. If $\tilde{G}_{(k)} > G_{(k)}$, then $|\tilde{G}_{(k)} - G_{(k)}| \leq |\tilde{G}_{(k)} - G_q| = |\tilde{G}_q - G_q| \leq \max_{1 \leq j \leq k} \{\|\hat{X}_j - X_j\|\} + \Delta$. Otherwise, $|\tilde{G}_{(k)} - G_{(k)}| \leq |\tilde{G}_p - G_p| \leq \max_{1 \leq j \leq k} \{\|\hat{X}_j - X_j\|\} + \Delta$. Now, $\Pr(\forall 1 \leq j \leq k : \|\hat{X}_j - X_j\| > \epsilon) \leq \sum_{j=1}^k \Pr(\|\hat{X}_j - X_j\| > \epsilon) \leq k \mathbf{E} \|\hat{X}_j - X_j\|^r \epsilon^{-r} = O(kn^{-r\beta}) = o(1)$ for a sufficiently large constant r . Therefore, $|\tilde{G}_{(k)} - G_{(k)}|$ converges to zero in probability, or $\tilde{G}_{(k)}$ converges to $G_{(k)}$ in probability. By Slutsky's lemma, $\log \tilde{G}_{(k)}$ converges to $\log G_{(k)}$ in probability and hence $I_1 = o_P(1)$.

For I_2 , we first observe that

$$I_2 = \left| \frac{1}{k-1} \sum_{j=1}^k \left(\log \tilde{G}_{(j)} - \log G_{(j)} \right) \right| = \left| \frac{1}{k-1} \sum_{j=1}^k \left(\log \tilde{G}_j - \log G_j \right) \right|.$$

By Markov's inequality, for any fixed $\epsilon > 0$,

$$\Pr(I_{21} > \epsilon) \leq \frac{\mathbf{E} I_{21}}{\epsilon} \leq \frac{k\mathbf{E} |\log \hat{G} - \log G|}{(k-1)\epsilon} = o(1),$$

where the last equality is obtained by Lemma S.7. We then deduce that $I_2 = o_P(1)$. Together with $I_1 = o_P(1)$ and (13), this implies that

$$\left| \frac{1}{k-1} \sum_{j=1}^{k-1} \log \frac{\hat{G}_{(k)} + \Delta}{\hat{G}_{(j)} + \Delta} - \frac{1}{k-1} \sum_{j=1}^{k-1} \log \frac{G_{(k)}}{G_{(j)}} \right| \rightarrow 0 \quad \text{in probability.}$$

Now we apply the argument in Levina and Bickel (2004) to conclude that \hat{d} is a consistent estimator.

(2) Let $h = h_{pca}$, and $\{\tilde{\phi}_k\}_{k=1}^d$ be a orthonormal basis system for $\iota_* T_x \mathcal{M}$ and $\{\psi_k\}_{k=1}^\infty$ be an orthonormal basis of \mathcal{L}^2 . Assume that \mathcal{M} is properly rotated and translated so that $\psi_k = \tilde{\phi}_k$ for $k = 1, 2, \dots, d$, and $x = 0 \in \mathcal{L}^2$. The sample covariance operator based on observations in $\hat{\mathcal{N}}_{\mathcal{L}^2}(h, x)$ is denoted by $\hat{\mathcal{C}}_x$ as in (6). It is seen that $\hat{\mathcal{C}}_x = n^{-1} \sum_{i=1}^n (\hat{X}_i - \hat{\mu}_x)(\hat{X}_i - \hat{\mu}_x)^* Z_i$, where $Z_i = 1_{\{\hat{X}_i \in \mathbb{B}_h^{\mathcal{L}^2}(x)\}}$ and $\hat{\mu}_x = n^{-1} \sum_{i=1}^n \hat{X}_i Z_i$. Let $\mathcal{H}_1 = \text{span}\{\psi_k : k = 1, 2, \dots, d\}$ and \mathcal{H}_2 be the complementary subspace of \mathcal{H}_1 in \mathcal{L}^2 , so that $\mathcal{L}^2 = \mathcal{H}_1 \oplus \mathcal{H}_2$. Let $\mathcal{P}_j : \mathcal{L}^2 \rightarrow \mathcal{H}_j$ be projection operators, and we define operator $\mathcal{A} = \mathcal{P}_1 \hat{\mathcal{C}}_x \mathcal{P}_1$, $\mathcal{B} = \mathcal{P}_2 \hat{\mathcal{C}}_x \mathcal{P}_2$, $\mathcal{D}_{12} = \mathcal{P}_1 \hat{\mathcal{C}}_x \mathcal{P}_2$ and $\mathcal{D}_{21} = \mathcal{P}_2 \hat{\mathcal{C}}_x \mathcal{P}_1$. Then $\hat{\mathcal{C}}_x = \mathcal{A} + \mathcal{B} + \mathcal{D}_{12} + \mathcal{D}_{21}$. Note that $\mathcal{D}_{12} + \mathcal{D}_{21}$ is self-adjoint. Therefore, if $y = \sum_{k=1}^\infty a_k \psi_k \in \mathcal{L}^2$,

$$\begin{aligned} \|\mathcal{D}_{12} + \mathcal{D}_{21}\|_{op} &= \sup_{\|y\|=1} \langle (\mathcal{D}_{12} + \mathcal{D}_{21})y, y \rangle = \sup_{\|y\|=1} \left(\langle \mathcal{P}_1 \hat{\mathcal{C}}_x \mathcal{P}_2 y, y \rangle + \langle \mathcal{P}_2 \hat{\mathcal{C}}_x \mathcal{P}_1 y, y \rangle \right) \\ &= 2 \sup_{\|y\|=1} \left(\sum_{k=d+1}^\infty \sum_{j=1}^d a_j a_k \langle \hat{\mathcal{C}}_x \psi_j, \psi_k \rangle \right) \leq 2 \sup_{\|y\|=1} \left(\sum_{k=d+1}^\infty \sum_{j=1}^d |a_j a_k| \cdot \left| \langle \hat{\mathcal{C}}_x \psi_j, \psi_k \rangle \right| \right) \\ &\leq 2 \sup_{j \leq d} \sup_{k \geq d+1} \left| \langle \hat{\mathcal{C}}_x \psi_j, \psi_k \rangle \right| \sup_{\|y\|=1} \left\{ \sum_{k=d+1}^\infty \sum_{j=1}^d (a_j^2 + a_k^2) \right\} \leq 2 \sup_{j \leq d} \sup_{k \geq d+1} \left| \langle \hat{\mathcal{C}}_x \psi_j, \psi_k \rangle \right|. \end{aligned}$$

From Lemma S.9, $\|\mathcal{D}_{12} + \mathcal{D}_{21}\|_{op} = O_P(h^{d+3} + n^{-1/2} h^{d/2+3} + n^{-\beta} h^{d+1})$. Similarly, we have $\|\mathcal{B}\|_{op} = O_P(h^{d+4} + n^{-1/2} h^{d/2+4} + n^{-\beta} h^{d+1})$, and $\mathcal{A} = \pi_{d-1} f(x) d^{-1} h^{d+2} \mathbf{I}_d + O_P(n^{-1/2} h^{d/2+2} + n^{-\beta} h^{d+1})$,

where π_{d-1} is the volume of $d-1$ dimensional unit sphere, and \mathbf{I}_d is the identity operator on \mathcal{H}_1 .

By assumption on ϱ , we have $\varrho < \min\{1/d, \beta\}$. Then h^{d+2} is the dominant term. Let $a_n = n^{-1/2}h^{-d/2}$ and $b_n = n^{-\beta}h^{-1}$, we have

$$\hat{\mathcal{C}}_x = \pi_{d-1}f(x)d^{-1}h^{d+2}\{\mathbf{I}_d + O_P(a_n + b_n)\tilde{\mathcal{A}} + O_P(h^2 + b_n)\tilde{\mathcal{B}} + O_P(h + b_n)(\tilde{\mathcal{D}}_{12} + \tilde{\mathcal{D}}_{21})\}$$

where $\tilde{\mathcal{A}}$, $\tilde{\mathcal{B}}$, $\tilde{\mathcal{D}}_{12}$ and $\tilde{\mathcal{D}}_{21}$ are all with operator norm equal to one, and $\tilde{\mathcal{D}}_{12}$ is the adjoint of $\tilde{\mathcal{D}}_{21}$. With the choice of ϱ , we have $\hat{\mathcal{C}}_x = \pi_{d-1}f(x)d^{-1}h^{d+2}\left\{\mathbf{I}_d + O_P(\sqrt{h})\tilde{\mathcal{A}} + O_P(h)\tilde{\mathcal{B}} + O_P(h)(\tilde{\mathcal{D}}_{12} + \tilde{\mathcal{D}}_{21})\right\}$. The same perturbation argument done in Singer and Wu (2012) leads to the desired result. \square

PROOF OF THEOREM 2. The proof is analogous to that of Theorem 4.2 of Cheng and Wu (2013), except that we need to handle the extra difficulty caused by noise on X . For clarity, we give a self-contained proof with emphasis on the extra issues. To reduce notions, let $h = h_{reg}$ and fix $x \in \mathcal{M} \setminus \mathcal{M}_{h_{reg}}$. Let $\{\hat{\varphi}_k\}_{k=1}^d$ be the orthonormal set determined by local FPCA and $\{\phi_k\}_{k=1}^d$ the associated orthonormal basis of $T_x\mathcal{M}$. Let $\{\psi_k\}_{k=1}^\infty$ be an orthonormal basis of \mathcal{L}^2 . Assume ι is properly rotated and translated so that $\iota(x) = 0 \in \mathcal{L}^2$ and $\psi_k = \iota_*\phi_k$ for $k = 1, 2, \dots, d$. Let $\mathbf{g} = (g(X_1), g(X_2), \dots, g(X_n))^T$. Then we have

$$\mathbf{E}\{\hat{g}(x) \mid \mathcal{X}\} = \mathbf{e}_1^T(\hat{\mathbf{X}}^T\hat{\mathbf{W}}\hat{\mathbf{X}})^{-1}\hat{\mathbf{X}}^T\hat{\mathbf{W}}\mathbf{g}.$$

Take $z = \exp_x(t\theta)$, where $t = O(h)$, $\|\theta\|_{\mathcal{L}^2} = 1$ and \exp_x denotes the exponential map at x . By Theorem 1, we have $\langle \iota_*\theta, \hat{\varphi}_k \rangle = \langle \iota_*\theta, \psi_k \rangle + O_P(h_{pca}^{3/2})$ and $\langle \Pi_x(\theta, \theta), \hat{\varphi}_k \rangle = O_P(h_{pca})$. By Lemma A.2.2. of Cheng and Wu (2013), we have

$$t\iota_*\theta = \iota(y) - t^2\Pi_x(\theta, \theta)/2 + O(t^3). \quad (14)$$

Therefore, for $k = 1, 2, \dots, d$, $\langle t\iota_*\theta, \psi_k \rangle = \langle t\iota_*\theta, \hat{\varphi}_k - O_P(h_{pca}^{3/2})\mathbf{u}_k \rangle = \langle \iota(z), \hat{\varphi}_k \rangle - t^2\langle \Pi_x(\theta, \theta), \hat{\varphi}_k \rangle/2 + O_P(hh_{pca}^{3/2} + h^2h_{pca}) = \langle \iota(z), \hat{\varphi}_k \rangle + O_P(hh_{pca}^{3/2} + h^2h_{pca})$. Since ι is an embedding, we have $\theta =$

$\sum_{k=1}^d \langle \iota_* \theta, \psi_k \rangle \phi_k$. Let $\mathbf{z} = (\langle \iota(z), \hat{\varphi}_1 \rangle, \langle \iota(z), \hat{\varphi}_2 \rangle, \dots, \langle \iota(z), \hat{\varphi}_d \rangle)^T$. By (14), it is easy to see that

$$\begin{aligned} g(x) - g(z) &= t\theta \nabla g(x) + \text{Hess } g(z)(\theta, \theta) t^2/2 + O_P(t^3) \\ &= \sum_{k=1}^d \langle t\iota_* \theta, \psi_k \rangle \nabla_{\phi_k} g(z) + \frac{1}{2} \sum_{j,k=1}^d \langle t\iota_* \theta, \psi_j \rangle \langle t\iota_* \theta, \psi_k \rangle \text{Hess } g(z)(\phi_j, \phi_k) + O_P(h^3) \\ &= \mathbf{z}^T \nabla g(x) + \frac{1}{2} \mathbf{z}^T \text{Hess } g(x) \mathbf{z} + O_P(h^{5/2}). \end{aligned}$$

Due to smoothness of g , compactness of \mathcal{M} and the compact support of K , we have $\mathbf{g} = \mathbf{X}[g(x) \ \nabla g(x)]^T + \mathbf{H}/2 + O_P(h^{5/2})$, where $\mathbf{H} = [\mathbf{x}_1^T \text{Hess } g(x) \mathbf{x}_1, \mathbf{x}_2^T \text{Hess } g(x) \mathbf{x}_2, \dots, \mathbf{x}_n^T \text{Hess } g(x) \mathbf{x}_n]^T$. Then the conditional bias is

$$\begin{aligned} \mathbf{E}\{\hat{g}(x) - g(x) \mid \mathcal{X}\} &= \mathbf{e}_1^T (\hat{\mathbf{X}}^T \hat{\mathbf{W}} \hat{\mathbf{X}})^{-1} \hat{\mathbf{X}}^T \hat{\mathbf{W}} \mathbf{g} - g(x) \\ &= \mathbf{e}_1^T \left(\frac{1}{n} \hat{\mathbf{X}}^T \hat{\mathbf{W}} \hat{\mathbf{X}} \right)^{-1} \frac{1}{n} \hat{\mathbf{X}}^T \hat{\mathbf{W}} (\mathbf{X} - \hat{\mathbf{X}}) \begin{bmatrix} g(x) \\ \nabla g(x) \end{bmatrix} \end{aligned} \quad (15)$$

$$+ \mathbf{e}_1^T \left(\frac{1}{n} \hat{\mathbf{X}}^T \hat{\mathbf{W}} \hat{\mathbf{X}} \right)^{-1} \frac{1}{n} \hat{\mathbf{X}}^T \hat{\mathbf{W}} \left\{ \frac{1}{2} \mathbf{H} + O_P(h^{5/2}) \right\}. \quad (16)$$

Now we analyze the term in (15). Let $Z = 1_{\hat{X} \in \mathbb{B}_h^{\mathcal{L}^2}(x)}$. By Lemma S.8, $\mathbf{E}Z \asymp h^d$. Then, by Hölder's inequality, for any fixed $\epsilon > 0$, we choose a constant $q > 1$ and a sufficiently large $p > 0$ so that $1/q + 1/p = 1$ and $\mathbf{E}Z \|\hat{X} - X\| = (\mathbf{E}Z)^{1/q} (\mathbf{E}\|\hat{X} - X\|^p)^{1/p} = O(h^{d-\epsilon d} n^{-\beta})$. Therefore,

$$\frac{1}{n} \hat{\mathbf{X}}^T \hat{\mathbf{W}} (\mathbf{X} - \hat{\mathbf{X}}) \begin{bmatrix} g(x) \\ \nabla g(x) \end{bmatrix} = \begin{bmatrix} \frac{1}{n} \sum_{i=1}^n K_h(\|\hat{X}_i - \iota(x)\|) (\mathbf{x}_i - \hat{\mathbf{x}}_i)^T \nabla g(x) \\ \frac{1}{n} \sum_{i=1}^n K_h(\|\hat{X}_i - \iota(x)\|) (\mathbf{x}_i - \hat{\mathbf{x}}_i)^T \nabla g(x) \hat{\mathbf{x}}_i \end{bmatrix} = O_P(h^{-1-\epsilon d} n^{-\beta}), \quad (17)$$

since

$$\begin{aligned} & \left| \frac{1}{n} \sum_{i=1}^n K_h(\|\hat{X}_i - \iota(x)\|) (\mathbf{x}_i - \hat{\mathbf{x}}_i)^T \nabla g(x) \right| \leq \frac{1}{n} \sum_{i=1}^n K_h(\|\hat{X}_i - \iota(x)\|) \|\mathbf{x}_i - \hat{\mathbf{x}}_i\|_{\mathbb{R}^d} \|\nabla g(x)\| \\ & \leq \{\sup_v |K(v)|\} \|\nabla g(x)\| \left(\frac{1}{n} \sum_{i=1}^n Z_i \|\mathbf{x}_i - \hat{\mathbf{x}}_i\|_{\mathbb{R}^d} \right) = O_P(h^{-1-\epsilon d} n^{-\beta}), \end{aligned}$$

and similarly, $n^{-1} \sum_{i=1}^n K_h(\|\hat{X}_i - x\|) (\mathbf{x}_i - \hat{\mathbf{x}}_i)^T \nabla g(x) \hat{\mathbf{x}}_i = O_P(h^{-1-\epsilon d} n^{-\beta}) \mathbf{1}_{d \times 1}$.

For $\hat{\mathbf{X}}^T \hat{\mathbf{W}} \hat{\mathbf{X}}$, a direct calculation shows that

$$\frac{1}{n} \hat{\mathbf{X}}^T \hat{\mathbf{W}} \hat{\mathbf{X}} = \begin{bmatrix} n^{-1} \sum_{i=1}^n K_h(\|\hat{X}_i - \iota(x)\|) & n^{-1} \sum_{i=1}^n K_h(\|\hat{X}_i - \iota(x)\|) \hat{\mathbf{x}}_i^T \\ n^{-1} \sum_{i=1}^n K_h(\|\hat{X}_i - \iota(x)\|) \hat{\mathbf{x}}_i & n^{-1} \sum_{i=1}^n \hat{\mathbf{x}}_i^T K_h(\|\hat{X}_i - \iota(x)\|) \hat{\mathbf{x}}_i \end{bmatrix}.$$

It is easy to check that $n^{-1} \sum_{i=1}^n K_h(\|\hat{X}_i - \iota(x)\|) = n^{-1} \sum_{i=1}^n K_h(\|X_i - \iota(x)\|) + O_P(h^{-1-\epsilon d} n^{-\beta})$, and note that the choice of h ensures that $h^{1+\epsilon d} \gg n^{-\beta}$. Similar calculation shows that $\frac{1}{n} \sum_{i=1}^n K_h(\|\hat{X}_i - \iota(x)\|) \hat{\mathbf{x}}_i^T = \frac{1}{n} \sum_{i=1}^n K_h(\|X_i - \iota(x)\|) \mathbf{x}_i^T + O_P(h^{-1-\epsilon d} n^{-\beta})$ and also $\frac{1}{n} \sum_{i=1}^n \hat{\mathbf{x}}_i^T K_h(\|\hat{X}_i - \iota(x)\|) \hat{\mathbf{x}}_i = \frac{1}{n} \sum_{i=1}^n \mathbf{x}_i^T K_h(\|X_i - x\|) \mathbf{x}_i + O_P(h^{-1-\epsilon d} n^{-\beta})$. Therefore,

$$\frac{1}{n} \hat{\mathbf{X}}^T \hat{\mathbf{W}} \hat{\mathbf{X}} = \frac{1}{n} \mathbf{X}^T \mathbf{W} \mathbf{X} + O_P(h^{-1-\epsilon d} n^{-\beta}) \mathbf{1}_{d \times 1} \mathbf{1}_{d \times 1}^T, \quad (18)$$

with

$$\frac{1}{n} \mathbf{X}^T \mathbf{W} \mathbf{X} = \begin{bmatrix} n^{-1} \sum_{i=1}^n K_h(\|X_i - x\|) & n^{-1} \sum_{i=1}^n K_h(\|X_i - x\|) \mathbf{x}_i^T \\ n^{-1} \sum_{i=1}^n K_h(\|X_i - x\|) \mathbf{x}_i & n^{-1} \sum_{i=1}^n \mathbf{x}_i K_h(\|X_i - x\|) \mathbf{x}_i^T \end{bmatrix}.$$

By Lemma S.4, S.5 and S.6, we have

$$\begin{aligned} & \frac{1}{n} \mathbf{X}^T \mathbf{W} \mathbf{X} \\ &= \begin{bmatrix} f(x) & h^2 u_{1,2} d^{-1} \nabla f(x)^T \\ h^2 u_{1,2} d^{-1} \nabla f(x) & h^2 u_{1,2} d^{-1} f(x) \mathbf{I}_d \end{bmatrix} + \begin{bmatrix} O(h^2) + O_P(n^{-\frac{1}{2}} h^{-\frac{d}{2}}) & O(h^3) + O_P(n^{-\frac{1}{2}} h^{-\frac{d}{2}+1}) \\ O(h^3) + O_P(n^{-\frac{1}{2}} h^{-\frac{d}{2}+1}) & O(h^{7/2}) + O_P(n^{-\frac{1}{2}} h^{-\frac{d}{2}+2}) \end{bmatrix}, \end{aligned}$$

where $u_{q,k}$ are constants defined in Section S.2 of Supplementary Material. Therefore, combined with (18), it yields

$$\begin{aligned} \frac{1}{n} \hat{\mathbf{X}}^T \hat{\mathbf{W}} \hat{\mathbf{X}} &= \begin{bmatrix} f(x) & h^2 u_{1,2} d^{-1} \nabla f(x)^T \\ h^2 u_{1,2} d^{-1} \nabla f(x) & h^2 u_{1,2} d^{-1} f(x) \mathbf{I}_d \end{bmatrix} \\ &+ \begin{bmatrix} O(h^2) + O_P(n^{-\frac{1}{2}} h^{-\frac{d}{2}}) + O_P(h^{-1-\epsilon d} n^{-\beta}) & O(h^3) + O_P(n^{-\frac{1}{2}} h^{-\frac{d}{2}+1}) + O_P(h^{-1-\epsilon d} n^{-\beta}) \\ O(h^3) + O_P(n^{-\frac{1}{2}} h^{-\frac{d}{2}+1}) + O_P(h^{-1-\epsilon d} n^{-\beta}) & O(h^{7/2}) + O_P(n^{-\frac{1}{2}} h^{-\frac{d}{2}+2}) + O_P(h^{-1-\epsilon d} n^{-\beta}) \end{bmatrix}. \end{aligned}$$

By our choice of h , we have $h^{-1-\epsilon d} n^{-\beta} \ll h^2$. Then, by binomial inverse theorem and matrix blockwise inversion, we have

$$\begin{aligned} \left(\frac{1}{n} \hat{\mathbf{X}}^T \hat{\mathbf{W}} \hat{\mathbf{X}} \right)^{-1} &= \begin{bmatrix} \frac{1}{f(x)} & -\frac{\nabla^T f(x)}{f(x)^2} \\ \frac{\nabla^T f(x)}{f(x)^2} & h^{-2} \frac{d}{u_{1,2} f(x)} \mathbf{I}_d \end{bmatrix} \\ &+ \begin{bmatrix} O_P(h^2 + h^{-1-\epsilon d} n^{-\beta} + n^{-\frac{1}{2}} h^{-\frac{d}{2}}) & O_P(h + h^{-3-\epsilon d} n^{-\beta} + n^{-\frac{1}{2}} h^{-\frac{d}{2}-1}) \\ O_P(h + h^{-3-\epsilon d} n^{-\beta} + n^{-\frac{1}{2}} h^{-\frac{d}{2}-1}) & O_P(h^{-\frac{1}{2}} + h^{-5-\epsilon d} n^{-\beta} + n^{-\frac{1}{2}} h^{-\frac{d}{2}-2}) \end{bmatrix}. \quad (19) \end{aligned}$$

Therefore, with (17), we conclude that

$$\mathbf{e}_1^T (\hat{\mathbf{X}}^T \hat{\mathbf{W}} \hat{\mathbf{X}})^{-1} \hat{\mathbf{X}}^T \hat{\mathbf{W}} \left\{ (\mathbf{X} - \hat{\mathbf{X}}) \begin{bmatrix} g(x) \\ \nabla g(x) \end{bmatrix} \right\} = O_P(h^{-1-\epsilon d} n^{-\beta}). \quad (20)$$

Now we analyze (16) with a focus on the term $\hat{\mathbf{X}}^T \hat{\mathbf{W}} \mathbf{H}$. A calculation similar to those in Lemma S.5 and S.6 shows that $\frac{1}{n} \sum_{i=1}^n K_h(\|X_i - \iota(x)\|) \mathbf{x}_i^T \text{Hess } g(x) \mathbf{x}_i = h^2 u_{1,2} d^{-1} f(x) \Delta g(x) + O_P(h^{7/2} + n^{-1/2} h^{-d/2+2})$ and $\frac{1}{n} \sum_{i=1}^n K_h(\|X_i - \iota(x)\|) \mathbf{x}_i^T \text{Hess } g(x) \mathbf{x}_i \mathbf{x}_i = O_P(h^4 + n^{-\frac{1}{2}} h^{-\frac{d}{2}+3})$. Therefore,

$$\frac{1}{n} \mathbf{X}^T \mathbf{W} \mathbf{H} = \begin{bmatrix} h^2 u_{1,2} d^{-1} f(x) \Delta g(x) + O_P(h^{7/2} + n^{-1/2} h^{-d/2+2}) \\ h^4 + n^{-\frac{1}{2}} h^{-\frac{d}{2}+3} \end{bmatrix}$$

and hence

$$\frac{1}{n} \hat{\mathbf{X}}^T \hat{\mathbf{W}} \mathbf{H} = \begin{bmatrix} h^2 u_{1,2} d^{-1} f(x) \Delta g(x) + O_P(h^{7/2} + n^{-1/2} h^{-d/2+2} + h^{-1-\epsilon d} n^{-\beta}) \\ O_P(h^4 + n^{-\frac{1}{2}} h^{-\frac{d}{2}+3} + h^{-1-\epsilon d} n^{-\beta}) \end{bmatrix}.$$

The choice of h implies that $n^{-\frac{1}{2}} h^{-\frac{d}{2}} \ll 1$. Thus, with (19), $\mathbf{e}_1^T (\hat{\mathbf{X}}^T \hat{\mathbf{W}} \hat{\mathbf{X}})^{-1} \hat{\mathbf{X}}^T \hat{\mathbf{W}} \left\{ \frac{1}{2} \mathbf{H} + O_P(h^3) \right\} = \frac{1}{2d} h^2 u_{1,2} \Delta g(x) + O_P(h^3 + n^{-\frac{1}{2}} h^{-\frac{d}{2}+2} + h^{-1-\epsilon d} n^{-\beta})$. Combining this equation with (16) and (20), we immediately see that the conditional bias is

$$\mathbf{E}\{\hat{g}(x) - g(x) \mid \mathcal{X}\} = \frac{1}{2d} h^2 u_{1,2} \Delta g(x) + O_P(h^3 + n^{-\frac{1}{2}} h^{-\frac{d}{2}+2} + h^{-1-\epsilon d} n^{-\beta}). \quad (21)$$

Now we analyze the conditional variance. Simple calculation shows that

$$\mathbf{Var}\{\hat{g}(x) \mid \mathcal{X}\} = n^{-1} \sigma_{\zeta}^2 \mathbf{e}_1^T (n^{-1} \hat{\mathbf{X}}^T \hat{\mathbf{W}} \hat{\mathbf{X}})^{-1} (n^{-1} \hat{\mathbf{X}}^T \hat{\mathbf{W}} \hat{\mathbf{W}} \hat{\mathbf{X}}) (n^{-1} \hat{\mathbf{X}}^T \hat{\mathbf{W}} \hat{\mathbf{X}})^{-1} \mathbf{e}_1^T. \quad (22)$$

It is easy to see that

$$\frac{1}{n} \hat{\mathbf{X}}^T \hat{\mathbf{W}} \hat{\mathbf{W}} \hat{\mathbf{X}} = \frac{1}{n} \mathbf{X}^T \mathbf{W} \mathbf{W} \mathbf{X} + O_P(n^{-\beta} h^{-d-1-\epsilon d}) \mathbf{1}_{(d+1) \times (d+1)}. \quad (23)$$

Also,

$$\frac{1}{n} \mathbf{X}^T \mathbf{W} \mathbf{W} \mathbf{X} = \begin{bmatrix} \frac{1}{n} \sum_{i=1}^n K_h^2(\|X_i - x\|) & \frac{1}{n} \sum_{i=1}^n K_h^2(\|X_i - x\|) \mathbf{x}_i^T \\ \frac{1}{n} \sum_{i=1}^n K_h^2(\|X_i - x\|) \mathbf{x}_i & \frac{1}{n} \sum_{i=1}^n K_h^2(\|X_i - x\|) \mathbf{x}_i \mathbf{x}_i^T \end{bmatrix}.$$

With Lemma S.4, S.5 and S.6, we can show that

$$\begin{aligned} & \frac{h^d}{n} \mathbf{X}^T \mathbf{W} \mathbf{W} \mathbf{X} \\ &= \begin{bmatrix} u_{2,0} \sigma^2 f(x) & h^2 d^{-1} u_{2,2} \sigma^2 \nabla f(x) \\ h^2 d^{-1} u_{2,2} \sigma^2 \nabla^T f(x) & h^2 d^{-1} u_{2,2} \sigma^2 f(x) \mathbf{I}_d \end{bmatrix} + \begin{bmatrix} O(h^2) + O_P(n^{-\frac{1}{2}} h^{-\frac{d}{2}}) & O_P(h^3 + n^{-\frac{1}{2}} h^{-\frac{d}{2}+1}) \\ O_P(h^3 + n^{-\frac{1}{2}} h^{-\frac{d}{2}+1}) & O_P(h^{\frac{7}{2}} + n^{-\frac{1}{2}} h^{-\frac{d}{2}+2}) \end{bmatrix}. \end{aligned}$$

Combined with (19), the above equation implies that

$$\begin{aligned} & n^{-1} \sigma_\epsilon^2 \mathbf{e}_1^T (n^{-1} \hat{\mathbf{X}}^T \hat{\mathbf{W}} \hat{\mathbf{X}})^{-1} (n^{-1} \mathbf{X}^T \mathbf{W} \mathbf{W} \mathbf{X}) (n^{-1} \hat{\mathbf{X}}^T \hat{\mathbf{W}} \hat{\mathbf{X}})^{-1} \mathbf{e}_1^T \\ &= \frac{1}{nh^d} \frac{u_{2,0} \sigma_\zeta^2}{f(x)} + O_P \left(n^{-1} h^{-d} (h^{-1-\epsilon d} n^{-\beta} + n^{-\frac{1}{2}} h^{-\frac{d}{2}}) \right). \end{aligned} \quad (24)$$

Also,

$$\begin{aligned} & n^{-1} \sigma_\zeta^2 \mathbf{e}_1^T (n^{-1} \hat{\mathbf{X}}^T \hat{\mathbf{W}} \hat{\mathbf{X}})^{-1} \mathbf{1}_{(d+1) \times (d+1)} (n^{-1} \hat{\mathbf{X}}^T \hat{\mathbf{W}} \hat{\mathbf{X}})^{-1} \mathbf{e}_1^T O_P (h^{-d-1-\epsilon d} n^{-\beta}) \\ &= O_P \left(n^{-\beta-1} h^{-d-1-\epsilon d} (1 + h + h^{-1-\epsilon d} n^{-\beta} + n^{-\frac{1}{2}} h^{-\frac{d}{2}-1}) \right). \end{aligned} \quad (25)$$

Combining the above result with (22), (23), (24), (25) and the fact $h^2 \geq h^{-1-\epsilon d} n^{-\beta}$ due to the choice of h , gives the conditional variance

$$\mathbf{Var}\{\hat{g}(x) \mid \mathcal{X}\} = \frac{1}{nh^d} \frac{u_{2,0} \sigma_\zeta^2}{f(x)} + O_P \left(n^{-1} h^{-d} (h + n^{-\frac{1}{2}} h^{-\frac{d}{2}}) \right). \quad (26)$$

Finally, the rate for $\mathbf{E}[\{\hat{g}(x) - g(x)\}^2 \mid \mathcal{X}]$ is derived from (21) and (26). \square

PROOF OF THEOREM 4. We first observe that

$$\mathbf{E} [\{\hat{g}(\tilde{x}) - g(x)\}^2 \mid \mathcal{X}] \leq 2\mathbf{E} [\{\hat{g}(\tilde{x}) - \hat{g}(x)\}^2 \mid \mathcal{X}] + 2\mathbf{E} [\{\hat{g}(x) - g(x)\}^2 \mid \mathcal{X}].$$

To derive the order for the first term, we shall point out that, with Lemma S.7, S.8 and S.9, by following almost the same lines of argument, conclusions of Theorem 1 hold for \tilde{x} . This means, by working on \tilde{x} instead of x , we still have a consistent estimate of dimension and a good estimate of tangent space at x . Given this, it is not difficult but somewhat tedious to verify that the argument in the proof of Theorem 2 and 3 still holds for \tilde{x} , with care for the discrepancy $\|\tilde{x} - x\|_{\mathcal{L}^2}$ instead of the discrepancy $\|\tilde{X}_i - X_i\|_{\mathcal{L}^2}$. This argument also shows that the order of the first term is the same as the second one (this is expected since \tilde{x} has the same contamination level of those \tilde{X}_i), and hence the conclusion of Theorem 4 follows. \square

References

ASWANI, A., BICKEL, P. and TOMLIN., C. (2011). Regression on manifolds: Estimation of the exterior derivative. *The Annals of Statistics* **39** 48–81.

CAI, T. and YUAN, M. (2011). Optimal estimation of the mean function based on discretely sampled functional data: Phase transition. *The Annals of Statistics* **39** 2330–2355.

CARDOT, H., FERRATY, F. and SARDA, P. (1999). Functional linear model. *Statistics & Probability Letters* **45** 11–22.

CARDOT, H. and SARDA, P. (2005). Estimation in generalized linear models for functional data via penalized likelihood. *Journal of Multivariate Analysis* **92** 24–41.

CHEN, D. and MÜLLER, H. (2012). Nonlinear manifold representations for functional data. *The Annals of Statistics* **40** 1–29.

CHENG, M. and WU, H. (2013). Local linear regression on manifolds and its geometric interpretation. *Journal of the American Statistical Association* **108** 1421–1434.

CORNEA, E., ZHU, H., KIM, P. and IBRAHIM, J. G. (2017). Regression models on Riemannian symmetric spaces. *Journal of the Royal Statistical Society, Series B* **79** 463–482.

DELAIGLE, A. and HALL, P. (2010). Defining probability density for a distribution of random functions. *The Annals of Statistics* **38** 1171–1193.

FAN, J. (1992). Design-adaptive nonparametric regression. *Journal of the American Statistical Association* **87** 998–1004.

FAN, J. (1993). Local linear regression smoothers and their minimax efficiencies. *The Annals of Statistics* **21** 196–216.

FERRATY, F., KEILEGOM, I. V. and VIEU, P. (2012). Regression when both response and predictor are functions. *Journal of Multivariate Analysis* **109** 10–28.

FERRATY, F. and VIEU, P. (2006). *Nonparametric Functional Data Analysis: Theory and Practice*. Springer-Verlag, New York.

GRONWALL, D. M. A. (1977). Paced auditory serial-addition task: A measure of recovery from concussion. *Perceptual and Motor Skills* **44** 367–373.

HALL, P. and HOROWITZ, J. L. (2007). Methodology and convergence rates for functional linear regression. *The Annals of Statistics* **35** 70–91.

HALL, P. and HOSSEINI-NASAB, M. (2006). On properties of functional principal components analysis. *Journal of the Royal Statistical Society: Series B (Statistical Methodology)* **68** 109–126.

HALL, P. and MARRON, J. S. (1997). On the shrinkage of local linear curve estimators. *Statistics and Computing* **516** 11–17.

HALL, P., MÜLLER, H. G. and WANG, J. L. (2006). Properties of principal component methods for functional and longitudinal data analysis. *The Annals of Statistics* **34** 1493–1517.

IBRAHIM, I., TINTERA, J., SKOCH, A., F., J., P., H., MARTINKOVA, P., ZVARA, K. and RASOVA, K. (2011). Fractional anisotropy and mean diffusivity in the corpus callosum of patients with multiple sclerosis: the effect of physiotherapy. *Neuroradiology* **53** 917–926.

JONGEN, P., TER HORST, A. and BRANDS, A. (2012). Cognitive impairment in multiple sclerosis. *Minerva Medica* **103** 73–96.

KONG, D., XUE, K., YAO, F. and ZHANG, H. H. (2016). Partially functional linear regression in high dimensions. *Biometrika* **103** 147–159.

KUDRASZOW, N. L. and VIEU, P. (2013). Uniform consistency of kNN regressors for functional variables. *Statistics & Probability Letters* **83** 1863–1870.

LANG, S. (1995). *Differential and Riemannian Manifolds*. Springer, New York.

LANG, S. (1999). *Fundamentals of Differential Geometry*. Springer, New York.

LEVINA, E. and BICKEL, P. (2004). Maximum likelihood estimation of intrinsic dimension. *Advances in Neural Information* **17** 777–784.

LI, Y. and HSING, T. (2010). Uniform convergence rates for nonparametric regression and principal component analysis in functional/longitudinal data. *The Annals of Statistics* **38** 3321–3351.

LILA, E. and ASTON, J. (2016). Smooth principal component analysis over two-dimensional man-

ifolds with an application to neuroimaging. *The Annals of Applied Statistics* **10** 1854–1879.

LOH, P.-L. and WAINWRIGHT, M. J. (2012). High-dimensional regression with noisy and missing data: Provable guarantees with non-convexity. *The Annals of Statistics* **40** 1637–1664.

MAS, A. (2012). Lower bound in regression for functional data by representation of small ball probabilities. *Electronic Journal of Statistics* **6** 1745–1778.

MÜLLER, H. G. and STADTMÜLLER, U. (2005). Generalized functional linear models. *The Annals of Statistics* **33** 774–805.

MÜLLER, H. G. and YAO, F. (2008). Functional additive models. *Journal of the American Statistical Association* **103** 1534–1544.

RAMSAY, J. O. and SILVERMAN, B. (2002). *Applied Functional Data Analysis: Methods and Case Studies*. Springer, New York.

RAMSAY, J. O. and SILVERMAN, B. W. (1997). *Functional Data Analysis*. Springer-Verlag, New York.

RAMSAY, J. O. and SILVERMAN, B. W. (2005). *Functional Data Analysis*. Springer Series in Statistics, 2nd edition. Springer, New York.

SEIFERT, B. and GASSER, T. (1996). Finite-sample variance of local polynomials: analysis and solutions. *Journal of the American Statistical Association* **91** 267–275.

SINGER, A. and WU, H.-T. (2012). Vector diffusion maps and the connection Laplacian. *Communications on Pure and Applied Mathematics* **65** 1067–1144.

STUELPNAGEL, J. (1964). On the parametrization of the three-dimensional rotation group. *SIAM Review* **6** 422–430.

TENENBAUM, J. B., DE SILVA, V. and LANGFORD, J. C. (2000). A global geometric framework for nonlinear dimensionality reduction. *Science* **290** 2319–2323.

TSYBAKOV, A. B. (2008). *Introduction to Nonparametric Estimation*. Springer, New York.

YAO, F. and MÜLLER, H. G. (2010). Functional quadratic regression. *Biometrika* **97** 49–64.

YAO, F., MÜLLER, H. G. and WANG, J.-L. (2005a). Functional data analysis for sparse longitu-

dinal data. *Journal of the American Statistical Association* **100** 577–590.

YAO, F., MÜLLER, H. G. and WANG, J.-L. (2005b). Functional linear regression analysis for longitudinal data. *The Annals of Statistics* **33** 2873–2903.

YUAN, M. and CAI, T. T. (2010). A reproducing kernel Hilbert space approach to functional linear regression. *The Annals of Statistics* **38** 3412–3444.

YUAN, Y., ZHU, H., LIN, W. and MARRON, J. S. (2012). Local polynomial regression for symmetric positive definite matrices. *Journal of Royal Statistical Society, Series B* **74** 697–719.

ZHANG, X. and WANG, J.-L. (2016). From sparse to dense functional data and beyond. *The Annals of Statistics* **44** 2281–2321.

ZHOU, L. and PAN, H. (2014). Principal component analysis of two-dimensional functional data. *Journal of Computational and Graphical Statistics* **23** 779–801.

